THE ASTROPHYSICAL JOURNAL, 479:388–397, 1997 April 10

A SEQUENCE OF OUTBURSTS FROM THE TRANSIENT X-RAY PULSAR GS 0834−430

COLLEEN A. WILSON, MARK H. FINGER,[1] B. ALAN HARMON, D. MATTHEW SCOTT,[2]
AND ROBERT B. WILSON
ES 84 Space Sciences Laboratory, NASA/Marshall Space Flight Center, Huntsville, AL 35812; wilsonc@gibson.msfc.nasa.gov, finger@gibson.msfc.nasa.gov, harmon@ssl.msfc.nasa.gov, scott@gibson.msfc.nasa.gov, wilson@gibson.msfc.nasa.gov

LARS BILDSTEN
Department of Physics and Department of Astronomy, University of California, Berkeley, CA 94720; bildsten@fire.berkeley.edu

AND

DEEPTO CHAKRABARTY[3] AND THOMAS A. PRINCE
Space Radiation Laboratory, California Institute of Technology, Pasadena, CA 91125; deepto@space.mit.edu, prince@thor.srl.caltech.edu
Received 1995 September 15; accepted 1996 October 2

ABSTRACT

GS 0834−430, a 12.3 s accretion-powered pulsar, has been observed in seven outbursts with the BATSE large-area detectors on the *Compton Gamma Ray Observatory*. The first five outbursts observed by BATSE occurred at intervals of about 107 days, while the final two outbursts were separated by about 140 days. The photon energy spectrum, measured by Earth occultation in the 20–100 keV band, can be fitted by a power law with photon index $\alpha \approx -3.7$ or by an exponential spectrum with temperature $kT \approx 15$ keV, with some variations within outbursts. The source has a low pulse fraction, $\lesssim 0.15$ in the 20–50 keV band. We have observed significant temporal and energy-dependent variations in epoch folded pulse profiles. Because the intrinsic torque effects for this system are at least comparable to orbital effects, pulse timing analysis did not produce a unique orbital solution. However, confidence regions for the orbital elements yielded the following 1 σ limits: orbital period $P_{\rm orb} = 105.8 \pm 0.4$ days and eccentricity $0.10 \lesssim e \lesssim 0.17$. GS 0834−430 is most likely a Be/X-ray binary.

Subject headings: binaries: general — pulsars: individual (PSR GS 0834−430) — stars: neutron — X-rays: stars

1. INTRODUCTION

GS 0834−430 is a transient X-ray pulsar first detected in outburst by *Granat*/WATCH in 1990 February (Lapshov et al. 1992a). The source was initially confused with the nearby X-ray burster MX 0836−42 (only 24′ away and also in outburst in 1990 February). Observations by *Ginga* (Aoki et al. 1992), *Granat*/ART-P (Sunyaev 1991), and *ROSAT* (Belloni et al. 1993) during later outbursts revealed a 12.3 s pulse period. The *ROSAT* observations (Belloni et al. 1993) determined the location of GS 0834−430 ($\alpha = 8^{\rm h}35^{\rm m}55\overset{\rm s}{.}1$, $\delta = -43°11'22''$, J2000) within a radius of 9″ (90% confidence). No optical counterpart has been identified.

WATCH observed six outbursts from GS 0834−430 between 1990 January and 1992 July with peak fluxes of 300–400 mcrab (8–20 keV). From these data, they derived an outburst period of about 110 days (Lapshov et al. 1992b). The observation of flux from GS 0834−430 in the 35-75 keV band by *Granat*/SIGMA (Denis et al. 1993), the presence of pulsations, and the regular outburst spacing suggested that this system could be a Be/X-ray binary. Although no outburst was observed by *Mir*/Kvant or BATSE at the expected time in 1992 November, *Mir*/Kvant observed a roughly constant flux of 20–30 mcrab in the 3–45 keV range from 1992 November 1–16 (Kaniovskii et al. 1994). The next outburst occurred about 30 days after the predicted time.

A total of 10 outbursts from GS 0834−430 have been observed since 1990 January. *Granat*/WATCH reported three outbursts prior to the launch of the *Compton Gamma Ray Observatory* (*CGRO*) in 1991 April. Since then, the *CGRO* Burst and Transient Source Experiment (BATSE) has observed seven outbursts through continuous monitoring using Earth occultation and epoch-folding analyses. The approximate outburst times determined by BATSE detection of pulsations are listed in Table 1. Also listed are times spanning observations by other instruments. For purposes of this paper we will number the outbursts 1–11, with No. 2 denoting the outburst that was not observed. BATSE has detected no significant outburst of GS 0834−430 since 1993 June.

A binary orbital period of 105.8 ± 0.4 days has been estimated from the BATSE timing data. The first five outbursts observed by BATSE (Nos. 5–9) occurred at a regular spacing of approximately 107 days, in agreement with the outburst period derived by the *Granat* team; however, the final two outbursts were spaced by about 140 days and were similar in intensity to the earlier outbursts. This behavior is unusual since Be/X-ray binaries typically outburst near periastron, resulting in regular orbitally modulated outbursts, or they have very large outbursts that are not related to the orbital phase (Waters et al. 1989). Interestingly, GS 0834−430 lies below the trend for Be/X-ray binaries on a spin versus orbital period diagram (Corbet 1986; Waters & van Kerkwijk 1989), in an otherwise "empty" region.

In this paper, we present the BATSE observations of GS 0834−430. Our observations include a light curve from 1991 April–1993 June, spectral analyses, and temporal and energy-dependent pulse profile variations. We perform a

[1] *CGRO* Science Support Center/ Goddard Space Flight Center.
[2] Universities Space Research Association.
[3] Current address: Center for Space Research, Massachusetts Institute of Technology, Cambridge, MA 02139.

TABLE 1

APPROXIMATE OUTBURST TIMES FOR GS 0834−430 OUTBURSTS OBSERVED BY BATSE[a]

Number	Start (MJD)	End (MJD)	Start (Calendar)	End (Calendar)	Instrument	Reference
1	47908	47965	1990 Jan 17	1990 Mar 15	*Granat*	1
3	48164	48182	1990 Sep 30	1990 Oct 18	*Granat*	1
3	48208	48208	1990 Nov 13	1990 Nov 13	*ROSAT*	2
3[b]	48222	48240	1990 Nov 27	1990 Dec 15	*Ginga*	3
4	48246	48293	1990 Dec 21	1991 Feb 6	*Granat*	1
4	48283	48285	1991 Jan 27	1991 Jan 29	*Ginga*	3
5	48374	48446	1991 Apr 28	1991 Jul 9	BATSE	
5	48381	48381	1991 May 5	1991 May 5	*ROSAT*	2
5	48397	48404	1991 May 21	1991 May 28	*Ginga*	3
6	48470	48542	1991 Aug 2	1991 Oct 13	BATSE	
6	48592	48535	1991 Aug 24	1991 Oct 6	*Granat*	1
7	48590	48644	1991 Nov 30	1992 Jan 23	BATSE	
7	48608	48609	1991 Dec 18	1991 Dec 19	SIGMA	4
8	48698	48761	1992 Mar 17	1992 May 19	BATSE	
9	48812	48842	1992 Jul 9	1992 Aug 8	BATSE	
9	48818	48828	1992 Jul 15	1992 Jul 25	*Granat*	1
[b]	48927	48950	1992 Nov 1	1992 Nov 24	*Mir*/Kvant	5
10	48950	48998	1992 Nov 24	1993 Jan 11	BATSE	
11	49101	49139	1993 May 24	1993 Jun 1	BATSE	

[a] Times spanning detections by other instruments are also included.

[b] Intraoutburst data is included in this interval.

REFERENCES.—(1) Lapshov et al. 1992a, 1992b; (2) Belloni et al. 1993; (3) Aoki et al. 1992; (4) Denis et al. 1993; (5) Kaniovskii et al. 1994.

pulse timing analysis and place constraints on the orbital parameters. We then discuss the implications of our results.

2. OBSERVATIONS AND ANALYSES

BATSE consists of eight identical uncollimated detectors positioned on the corners of the *CGRO* spacecraft such that the normal vectors of the detectors are perpendicular to the faces of a regular octahedron. The data presented here were taken with the BATSE large-area detectors (LADs), which are Na I (Tl) scintillation crystals with a geometric area of 2025 cm^2 and a thickness of 1.27 cm. The LADs are sensitive to photons from 20 to 1800 keV. The lack of collimation allows maximum sky coverage for transient and burstlike events. Two BATSE data types were used in this analysis, the CONT (2.048 s, 16 channel) data and the DISCLA (1.024 s, 4 channel) data. The DISCLA data were used for pulse arrival time analysis. The CONT data were used for spectral fitting, flux and pulse fraction determination, and pulse profile analysis. A more complete description of the instrument and data types can be found in Fishman et al. (1989).

2.1. *Source Flux Measurements Using Earth Occultation*

The intensity of a known source is measured by calculating the difference in total count rate in source-facing detectors just before and after source occultation by Earth. Using this technique, BATSE has monitored the flux at the location of GS 0834−430 continuously since 1991 April. To generate the light curve, source count rates were measured twice per *CGRO* orbit using 16 channel 2.048 s time resolution CONT data (Harmon et al. 1992). Two minutes of data immediately before and after an occultation step were fitted with a quadratic background plus a steplike function defined by the atmospheric attenuation along the line-of-sight to the source. Additional terms in the fit were included for occultation steps of known bright sources within the fit window. If these bright source steps occurred within 10 s of the step being measured, that step was not used. Gamma-ray bursts, solar flares, South Atlantic Anomaly passages, and electron precipitation events also reduced the number of usable steps. Typically, about 10–15 clean steps per day were available for monitoring GS 0834−430. When the angle between the *CGRO* orbital plane and the source (β angle) approached 70° (the Earth half-angle), the occultations broadened and then ceased (Harmon et al. 1992). Every 52 days (*CGRO* orbital precession period), the 28°.5 *CGRO* orbital inclination angle and the −43° declination of GS 0834−430 combined to a maximum β greater than 70°, so that the source was not occulted for an interval of 3 days.

Some interfering sources introduced additional complications to the measurement of GS 0834−430. Figure 1 shows the projections of the limb of Earth at a typical time of GS 0834−430 rise and set. Detectable sources that are

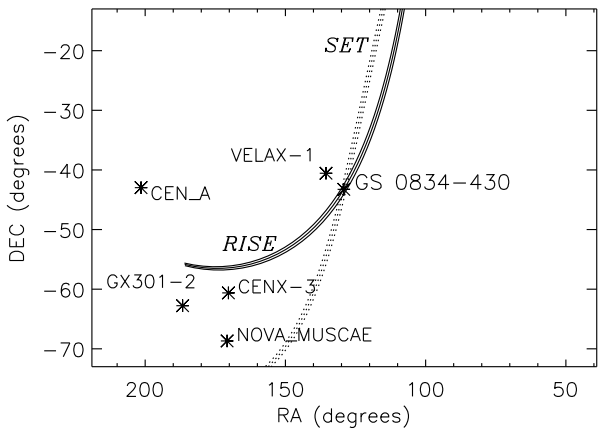

FIG. 1.—Nearby sources to GS 0834−430. These sources are variable and have occultation times that often occur within the step fitting window. The solid curve represents the rising occultation limb ±10 s. The dotted curve represents the setting occultation limb ±10 s. The limbs change according to spacecraft pointings. At some time during observations of GS 0834−430, an occultation limb for each of the sources shown was within 2° of the GS 0834−430 limbs.

near GS 0834−430 are also shown. At intervals equal to the spacecraft precession period, the angles between these sources and the GS 0834−430 occulting limb became small. An example of the motion of occultation limbs with time can be found in McNamara, Harmon, & Harrison (1995). Individual steps where the limb separations were less than 2° were removed from the flux calculation. This provided a more stringent requirement on the data than the 10 s limit mentioned earlier. From 1992 August 3–1993 May 22 (MJD 48840–49100), steps where the limb separation between GS 0834−430 and the very bright transient, GRO J0422+32 (Callanan et al. 1995) was less than 5° were removed.

Vela X-1 presented an additional problem because it has very bright episodes, is only 6° away from GS 0834−430, and has a 283 s pulse period which is of the same order as the step fitting time interval. The long pulse period introduced steep slopes (which are correlated with occultation step size) and relatively short timescale features into the background. In an attempt to remove Vela X-1 more completely, the fit window was extended to 285 s on either side of the GS 0834−430 step and a Vela X-1 template term was included, which was obtained from fitting phases in the 20–50 keV band of BATSE DISCLA data for Vela X-1. This method was unsuccessful because it increased the systematic errors and residuals from pulse shape variations that remained in the data. Most of the effects from Vela X-1 were removed by averaging standard data over 10 day intervals. In addition, outliers that appeared to be associated with bright episodes of Vela X-1 were removed.

Occultation measurements from eight energy channels (20–160 keV) were averaged over 3 days during GS 0834−430 outbursts and were fitted by a photon power law with varying photon index and amplitude. The photon index varied from −3.0 to −4.4 around an average value of $\alpha \approx -3.7$ and showed no significant trends with intensity. The large range of values for α was most likely due to the fact that the spectrum was usually constrained by only three or four energy channels, so variations in individual channels could have affected the spectral fits. The same data were also fitted with an exponential model,

$$\frac{dN}{dE} = \frac{A}{E} \exp\left(\frac{-E}{kT}\right), \quad (1)$$

with varying temperature kT and amplitude A. The temperature varied from 12 to 18 keV around an average value $kT \approx 15$ keV and also showed no significant trends. Again, the large range was most likely due to a poorly constrained spectrum rather than variations intrinsic to the source. Both models were acceptable fits to the data and produced equivalent flux estimates. In Figure 2 the *Ginga* spectral model from 1991 May 28 (Aoki et al. 1992) has been overlaid with the near simultaneous BATSE data and model. The BATSE spectral model is a power law with a photon index, $\alpha = -3.8 \pm 0.4$. The BATSE and *Ginga* spectral models show good agreement. To calculate a bolometric correction to the BATSE data, the *Ginga* model was integrated from 2–30 keV and the BATSE model was integrated from 30–100 keV. The total (2–100 keV) energy flux was 3.5 times the BATSE energy flux.

In Figure 3, fluxes were generated by fitting 10 day average source count rates with a power law with a fixed photon index, $\alpha = -3.7$. The model was then integrated from 20–100 keV. The flux values peaked at about 300 mcrab (where 1 mcrab = 3.1×10^{-4} photons cm^{-2} s^{-1} in the 20–100 keV band) and fell to 30–50 mcrab between outbursts. Upper limits of 10 mcrab were observed for the GS 0834−430 location since the outbursts ceased. Hence, much of the observed intraoutburst flux was apparently due to GS 0834−430 plus a small fraction from interfering sources. An overall decline in the peak flux can be seen for the first five outbursts (Nos. 5–9). However, the next outburst (No. 10), which occurred just after the spacing between outbursts increased significantly, was comparable in brightness to the first outburst. In addition, a decline in the width (as measured by a Gaussian fit to each outburst) of the first five outbursts (Nos. 5–9) was observed.

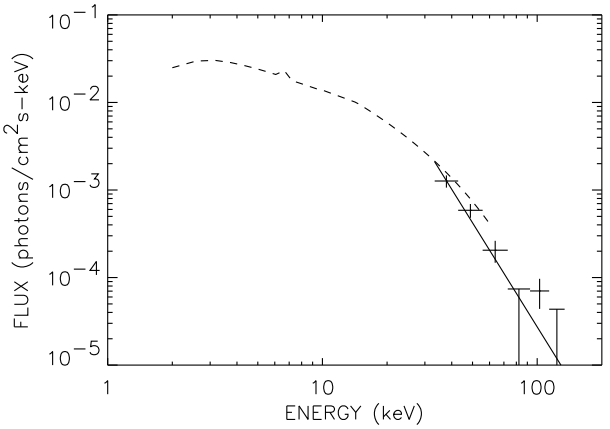

FIG. 2.—Combined BATSE and *Ginga* spectrum for 1991 May 28. The dotted line is the *Ginga* model spectrum (Aoki et al. 1992), and the solid line is the BATSE model spectrum. BATSE data points are given by horizontal bars that are the width of the energy bins. A bolometric correction, $F_{\rm total} = 3.5F_{\rm BATSE}$, to the BATSE 30–100 keV data was calculated from this spectrum.

Systematic errors in the occultation method were estimated from about 700 days of flux measurements, 1993 July–1995 May, when GS 0834−430 was not detected by

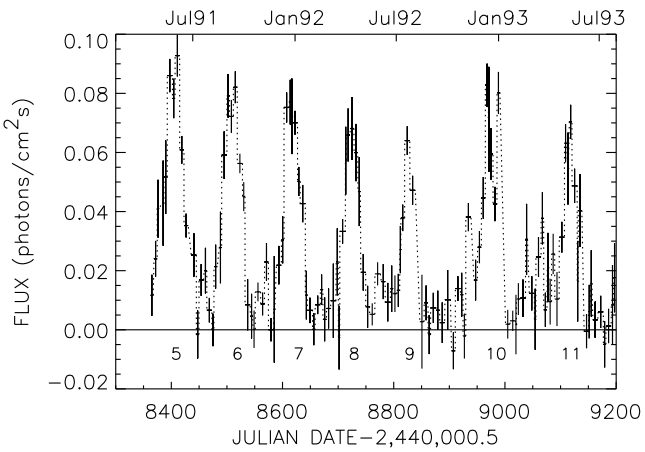

FIG. 3.—GS 0834−430 flux history in Earth occultation data (20–100 keV), generated by fitting a power law with a fixed spectral photon index $\alpha = -3.7$ to 10 day average count rates. The error bars shown in the figure have been multiplied by 1.65 to include systematic error. The increased scatter in the data from days 8840–9100 is caused by flickering of the bright transient GRO J0422+32 during outburst (Callanan et al. 1995). BATSE has observed no outburst from GS 0834−430 since 1993 June.

BATSE. The significances of these fluxes were binned into a histogram and the variance, σ^2, of this distribution was calculated. For a Gaussian distribution with no systematic error, $\sigma = 1$. For the 700 days used, a σ of 1.65 was obtained. The error bars in Figure 3 have been multiplied by 1.65 to include systematic errors.

The flux data, with errors including systematic errors, were folded at periods ranging from 1 to 200 days. A χ^2 value for a constant at each period was calculated. In Figure 4*a*, the period search results for the first five outbursts (Nos. 5–9) are shown. A strong peak is located at 107.1 ± 0.4 days, and a smaller peak can be seen at half that value. However, in Figure 4*b*, the period search results for the last three outbursts (Nos. 9–11), no peak is observed at 107 days; although a broad enhancement exists near 140 days and a smaller enhancement occurs at half that value. If all seven outbursts are folded, the peak in χ^2 is located at 109.9 ± 0.5 days. The 107.1 day outburst profile for the first five outbursts is shown versus arbitrary phase in Figure 4*c*. The outburst profile has no large asymmetries, as also observed by *Granat* (Lapshov et al. 1992b). A power spectrum analysis was also performed on this data set. This produced peaks at 105.3 ± 0.9 days for the first five outbursts and 114.7 ± 1.1 days for all seven outbursts (Robinson 1996).

2.2. *Pulsed Observations*

2.2.1. *Epoch-folding Analysis and Period History*

An epoch-folding analysis of the 20–50 keV DISCLA data was performed for the 800 days containing seven outbursts of GS 0834−430. In this analysis, data were rejected when GS 0834−430 was occulted by Earth, or when solar flares, gamma-ray bursts, or other events caused rapid variations in the counting rates. The count rates were then summed over the detectors exposed to GS 0834−430, with a weighting for each detector given by the cosine of the aspect angle. Data in 0.5 day intervals were fitted to a model in which the pulse source flux was represented by a fifth-order harmonic expansion in the pulsar phase. Higher order terms were neglected because they could not be measured with the 1.024 s resolution DISCLA data. To represent the background, the intervals were divided into 300 s segments, and the background in each segment was modeled as a quadratic in time. The background model value and slope were constrained to be continuous at segment boundaries. In the calculation of pulse phases from folding the DISCLA data, pulse arrival times were corrected to the solar system barycenter using the planetary ephemeris Jet Propulsion Laboratory DE-200 (Standish et al. 1992), a preliminary binary ephemeris (Wilson et al. 1994), and a pulsar rest frame phase model. A pulse template was obtained from folding the DISCLA data during a strong outburst, subtracting the mean, and normalizing to obtain a mean square value of 1. The 527 parameterized pulse profiles obtained from the 0.5 day interval fits were then correlated with the pulse template to obtain a GS 0834−430 pulse intensity and the phase offset from the preliminary ephemeris for each interval. Variations of the pulse shape with time and their effects on model fits are discussed in § 2.2.3.

Figure 5 shows the barycentered pulse period history measured by BATSE and the measured periods obtained by *Granat* (Sunyaev 1991; Grebenev & Sunyaev 1991; Sunyaev et al. 1992), *Ginga* (Aoki et al. 1992), and *ROSAT* (Belloni et al. 1993). Three-day intervals of phase offsets generated without assuming a binary ephemeris were fitted by first-order polynomials to obtain the periods in the plot. An orbital signature is strongly suggested by the presence of spin-up and spin-down trends within outbursts.

2.2.2. *Model Fitting and Orbital Constraints*

The phase data were fitted with a binary orbit model plus a global polynomial $\dot{\nu}$ model. For a first-order polynomial in $\dot{\nu}$, a reduced chi-squared value of $\chi^2_\nu = 809$ was obtained. For higher order polynomials, e.g., seventh-order, $\chi^2_\nu \gtrsim 50$. Clearly, such a model for the spin-up rate was too simple. Next, ϕ was represented by an orbit plus a different polynomial in each outburst. For emission times $t_k^{\rm em}$ within the

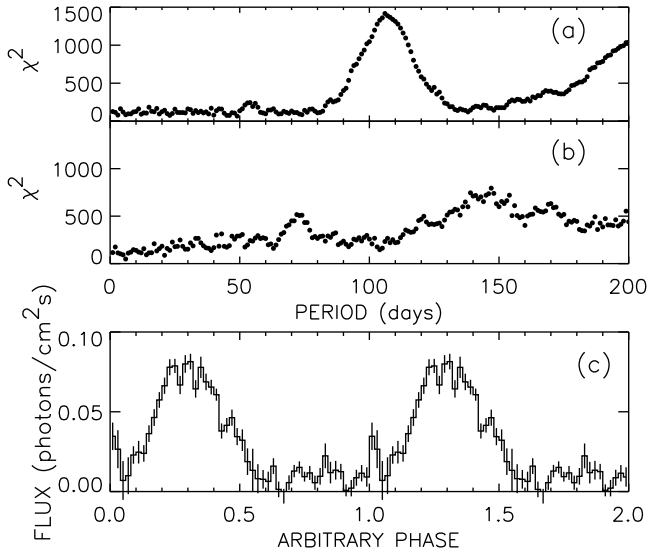

FIG. 4.—A one-day average flux history was folded at periods ranging from 1 to 200 days. A χ^2 test was performed, comparing the folded data at each period to a constant value. Data folded for the first five outbursts, (*a*) 1991 April–1992 August, shows a strong peak at 107.1 ± 0.4 days. However, data folded for the last three outbursts, (*b*) 1992 July–1993 June, shows no strong peaks. (*c*) 107.1 day folded outburst profile for 1991 April–1992 August.

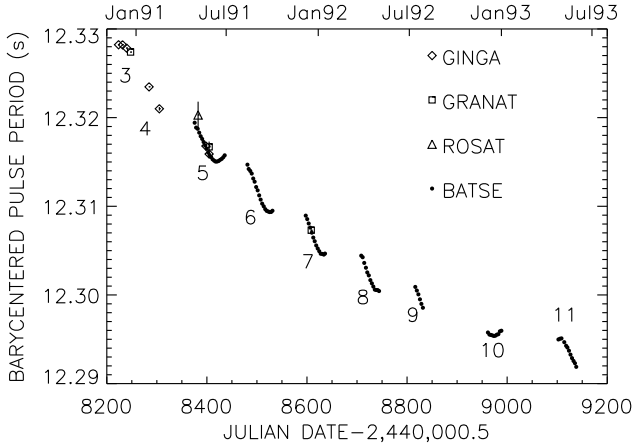

FIG. 5.—Pulse period history of GS 0834−430, corrected to the solar system barycenter, with no binary orbital corrections included. Period measurements from *Granat* (Sunyaev 1991; Grebenev & Sunyaev 1991; Sunyaev et al. 1992), *Ginga* (Aoki et al. 1992), and *ROSAT* (Belloni et al. 1993) are also shown.

ith outburst,

$$\phi^{\rm model}(t_k^{\rm em}) = \phi_{o_i} + \nu_{o_i}(t_k^{\rm em} - \tau_i) + \int_{\tau_i}^{t_k{\rm em}} \dot{\nu}_i^{\rm model}(t')(t_k^{\rm em} - t')dt' \ , \tag{2}$$

where i denotes the outburst number, $t_k^{\rm em}$ is a pulse emission time, τ_i is a fixed reference epoch in outburst i, and ϕ_{o_i} and ν_{o_i} are adjustable phase and spin frequency at epoch τ_i, and

$$\dot{\nu}_i^{\rm model} = \sum_{j=0}^{N} \frac{d^{(j+1)}\nu}{dt^{(j+1)}} \frac{(t_k^{\rm em} - \tau_i)^j}{j!} \ , \tag{3}$$

where $d^{(j+1)}\nu/dt^{(j+1)}$ are adjustable parameters at epoch τ_i. First, an orbit was fixed and the number of terms increased in each outburst until χ^2 reached a minimum. Since the minimum reduced $\chi_\nu^2 = 1.24$ at $N = 6$, we treated this as a measure of noise in excess of counting statistics in the phases and increased the phase errors by $(1.24)^{1/2}$ to compensate. Next, an orbit and a different quadratic ($N = 2$) $\dot{\nu}^{\rm model}$ were fitted to each outburst, with all parameters allowed to vary. The fit χ^2 is written as

$$\chi^2 = \sum_{k=1}^{N} \frac{[\phi_k - \phi^{\rm model}(t_k^{\rm em})]^2}{\sigma_{\phi k}^2} \tag{4}$$

for the phase measurements ϕ_k which have errors $\sigma_{\phi k}$. The phase model $\phi^{\rm model}$ is evaluated at the emission time $t_k^{\rm em}$ which depends upon both the barycentric observation time and the adjustable binary ephemeris parameters. The fit converged to a reduced $\chi_\nu^2 = 1.1$ for 487 degrees of freedom, but $a_{\rm X}$ sin i, e, and ω were poorly determined. The value a is the semimajor axis, i is the angle between the orbital angular momentum vector and the line of sight, e is the eccentricity, and ω is the longitude of periapse. The parameters of this minimum χ^2 value are shown in Table 2. The errors on the parameters are 68% single parameter confidence intervals (Lampton, Margon, & Bowyer 1976). Figure 6 shows the measured phases, model components, and phase residuals for this model. Figure 7 shows the intrinsic $\dot{\nu}$ model. One must keep in mind that this is the minimum χ^2 solution, an example from a large family possible solutions. The $\dot{\nu}$ model is constrained only by the data. However, the presence of a peak in $\dot{\nu}$ within outbursts, the lack of any global trends, and the concentration of spin-up within outbursts strongly suggest that the outburst mechanism is variable accretion, not obscuration. Variable accretion is the mechanism believed to power Be/X-ray binary systems.

Since $a_{\rm X}$ sin i and e were not well determined, two-parameter confidence regions were examined to constrain these parameters. Figure 8 shows confidence regions for $a_{\rm X}$ sin i and $ea_{\rm X}$ sin i. The levels shown are 68%, 90%, and 99%, respectively. Figure 8 shows that although $a_{\rm X}$ sin i is not well constrained by the data, $ea_{\rm X}$ sin i is. The pulse

TABLE 2

MODEL FITTING RESULTS AT $\chi^2_{\rm min}$ [a]

Parameter	Value
χ^2 (dof)	534.9(487)
$P_{\rm orb}$ days	105.8 ± 0.4
τ_2	JD $2448810.1^{+1.6}_{-1.4}$
$a_{\rm X}$ sin i lt-s	128^{+47}_{-38}
$ea_{\rm X}$ sin i lt-s	$15.3^{+3.3}_{-0.9}$
ω°	140^{+35}_{-53}
$f(M)$	$0.20^{+0.30}_{-0.10}$

[a] Errors are calculated from 68% single parameter confidence levels.

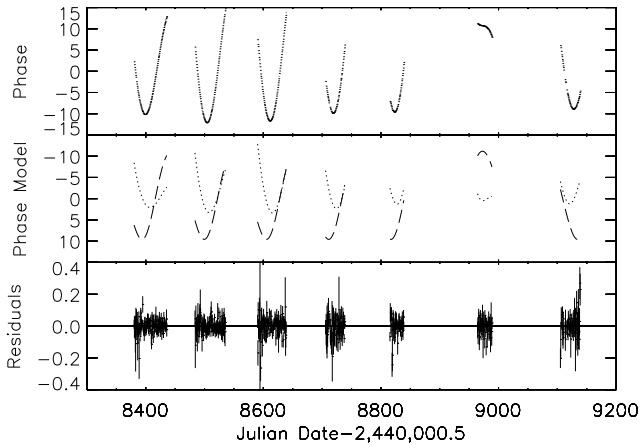

FIG. 6.—Top panel contains the phase points from outbursts Nos. 5–11 measured by BATSE. The center panel is the two model components of the phase model described in § 2.2.2. The dotted line is the intrinsic torque component, and the dashed line is the orbital component. The bottom panel shows the phase residuals for this model.

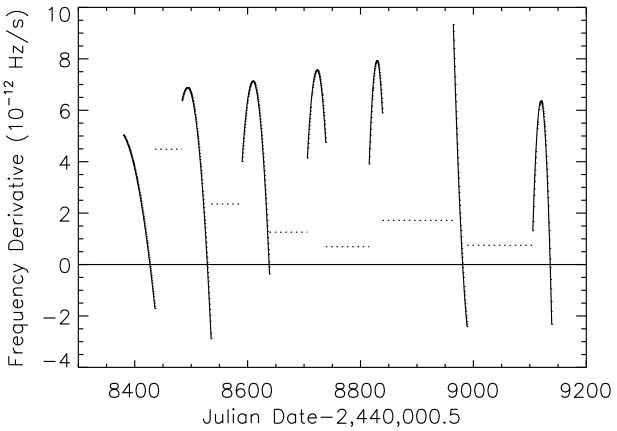

FIG. 7.—Intrinsic $\dot{\nu}$ model evaluated at the minimum χ^2 described in § 2.2.2. This is an example of $\dot{\nu}$ behavior extracted from a large family of allowable solutions. The dotted lines are calculated $\dot{\nu}$ values between outbursts.

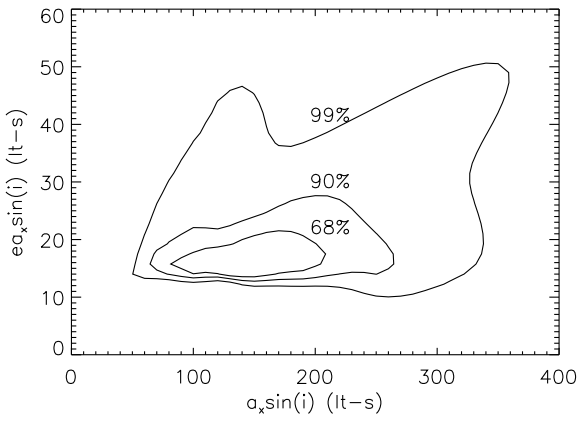

FIG. 8.—Constraints on $a_{\rm X}$ sin i and $ea_{\rm X}$ sin i. Contours shown are 68%, 90%, and 99% confidence levels.

arrival time delay due to a binary orbit is given by (Deeter, Boynton, & Pravdo 1981),

$$z = a_X \sin i \sin (M + \omega) + \tfrac{1}{2} e a_X \sin i \sin (2M + \omega) - \tfrac{3}{2} e \cos \omega + O(e^2) , \quad (5)$$

where M is the mean anomaly. This is used to calculate the pulse emission time $t_j^{em} = t_j^{SSB} - z$, where t_j^{SSB} is the pulse arrival time at the solar system barycenter. We note that the second term in equation (5) is much better constrained by the phase data than the first.

Next, the values of τ_p, the epoch of periastron passage, and ω, the periapse angle, that resulted from the fits within the confidence intervals were compared. These two parameters were highly correlated as expected, so a new epoch called τ_2 was defined. From the second term above,

$$2M + \omega = \frac{4\pi}{P_{orb}} (t - \tau_2) , \quad (6)$$

where

$$\tau_2 = \left(\tau_p - \frac{\omega P_{orb}}{4\pi} \right) \quad (7)$$

and P_{orb} is the orbital period. Note that τ_2 repeats with a cycle of P_{orb} or $\omega + 4\pi$. Two-parameter confidence regions were examined for τ_2 and ω. The results of this analysis are shown in Figure 9. Again the levels shown are 68%, 90%, and 99% confidence, respectively. The plot spans more than 360° because τ_2 has a 4π cycle.

Next, we attempted to extract more information about the system by replacing $a_X \sin i$ with the mass function,

$$f(M) = \frac{4\pi^2 (a_X \sin i)^3}{G P_{orb}^2} . \quad (8)$$

We then examined two-parameter confidence regions in e and $f(M)$. Figure 10 shows that to allow a large mass function which would be expected for a Be companion, $0.04 < e < 0.2$, unless the inclination is quite small. If the eccentricity is more typical of a Be/X-ray binary ($0.2 < e < 0.4$), then $f(M) < 0.5$.

We have reached several conclusions. The second term in equation (5) is well constrained by the data, while the first term is not. A circular orbit appears to be ruled out (see Fig. 8). Three of the five orbital parameters (P_{orb}, τ_2, and $ea_X \sin i$) are well known, but $a_X \sin i$ and ω are poorly known.

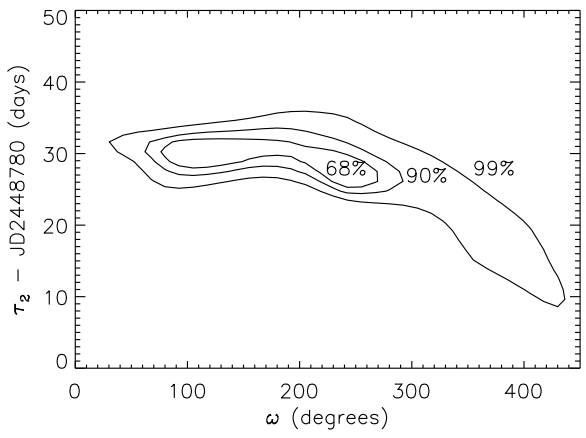

FIG. 9.—Constraints on τ_2 and ω. Contours shown are 68%, 90%, and 99% confidence levels.

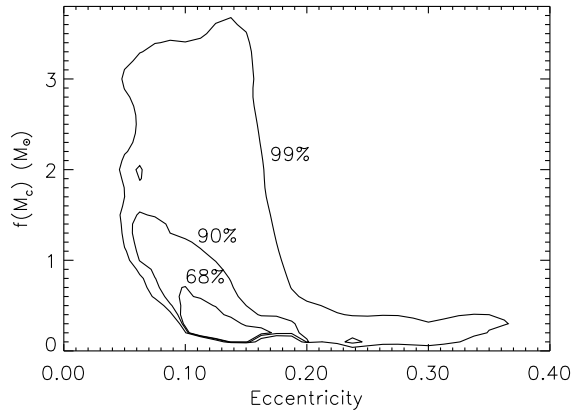

FIG. 10.—Constraints on $f(M_c)$ and e. Contours shown are 68%, 90%, and 99% confidence levels.

2.2.3. *Pulse Profile Variations*

As shown in Figure 11 the GS 0834−430 pulse profile consists of multiple components which vary considerably from one energy band to another. The pulse profiles shown are limited to the first three harmonics to minimize noise contributions. The error bars are spaced such that individual points are uncorrelated. The leading component (≈phase 0.3–0.75) appears to be dominant or at least equivalent in the 20–30 keV band, while the trailing component (≈phase 0.75–0.3) is dominant at higher energies. Pulse profiles observed by BATSE are similar to those observed by *Ginga* in the 1.2–27.5 keV range (Aoki et al. 1992). Both BATSE and *Ginga* observed significant pulse shape variations with energy. The pulse profiles from different time intervals are not phase aligned. Hence any shift in phase between the different time intervals shown in Figure 11 is arbitrary; however, the apparent shift in phase of profile features between different energy bands within a single time interval is intrinsic to the source.

CONT data were folded to obtain pulse profiles. The phase model used consisted of a quadratic and an orbital model obtained from DISCLA data. Due to the large intrinsic $\dot{\nu}$, which was not simply behaved, only short ($\lesssim$2 weeks)

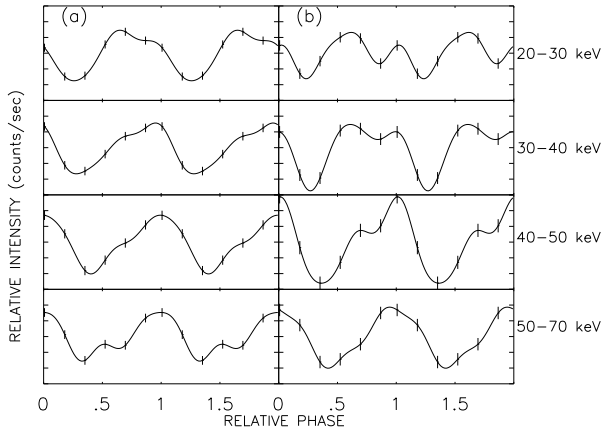

FIG. 11.—(*a*) Pulse profile from outburst No. 6, 1991 September 19–23 (MJD 48518–48522), used as the first template in temporal pulse shape variations analysis. (*b*) Pulse profile from outburst No. 7, 1991 December 28–1992 January 2 (MJD 48618–48622).

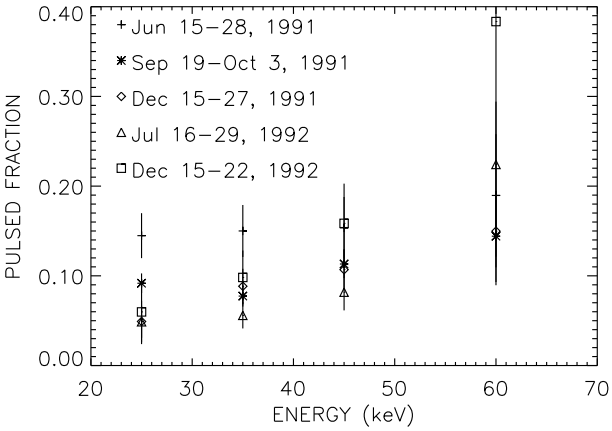

FIG. 12.—Pulse fraction calculations for GS 0834−430, using $(\bar{r}_{\rm pulsed} - r_{\rm pulsed_{min}})/r_{\rm occ}$, where r is the count rate.

intervals were used to minimize smearing in individual pulse profiles. Any trends remaining in the phase residuals were removed by fitting 1 day bins with a quadratic which was then used to correct the pulse profiles.

The algorithm used to compute pulse profiles introduced correlations between adjacent phase bins, making a statistical comparison of different pulse profiles difficult to correctly formulate in the time domain (see Appendix). However, such a comparison is easily formulated in the frequency domain. As shown in the Appendix, the harmonic coefficients of the pulse profile are uncorrelated (although their errors are dependent upon harmonic number). These harmonic coefficients were calculated as

$$a_k = \frac{1}{N} \sum_{j=1}^{N} R_j e^{-2\pi i jk/N} , \tag{9}$$

where $i = (-1)^{1/2}$, $N = 64$ is the number of phase bins, and R_j is the count rate in the jth bin of the pulse profile. Only the first three harmonics were kept because higher order harmonics were not statistically significant. The variance on the harmonic coefficients of order k is

$$\sigma^2_{\mathbf{Re}\,(a_k)} = \frac{b_k}{2} \frac{1}{N^2} \sum_{j=1}^{N} \sigma^2_{R_j} , \tag{10}$$

where $\sigma^2_{R_j}$ is the variance of R_j and b_k is a correction due to the rebinning. A detailed derivation of b_k is given in the Appendix.

A study of pulse profiles from all seven outbursts observed by BATSE has resulted in the discovery of two different pulse shapes. For this analysis, harmonic representations of 3–6 day summed pulse profiles were compared. The time interval lengths were chosen to maximize signal, while minimizing phase drift. Only the first three harmonics were considered in the analysis because the higher harmonics were not statistically significant. A template was chosen from the set of pulse profiles, and it was compared to all available profiles by minimizing

$$\chi^2 = \sum_{c=1}^{4} \sum_{k=1}^{3} \frac{|\, a_k^c - t_k^c \beta_c e^{2\pi i \phi k} \,|^2}{[\sigma^c_{\mathbf{Re}\,(a_k c)}]^2 + \beta_c^2 [\sigma^c_{\mathbf{Re}\,(t_k c)}]^2} , \tag{11}$$

where k is the harmonic number, c is the energy channel number, t_k^c is the harmonic coefficient of the template profile for channel c, a_k^c is the harmonic coefficient of the compared profile for channel c, ϕ is a phase factor common to all energy channels, and β_c is an energy channel–dependent scaling factor. The time interval from 1991 September 19–23 (Fig. 11*a*) was chosen as the initial template and compared in each energy channel with 40 intervals spanning the seven outbursts. Intervals with significant signals in less than three energy channels were not included in the comparisons. Of the 40 intervals studied, three showed significant deviations from the template at the 99% confidence level. Next, the most significantly different interval, 1991 December 28–1992 January 2, shown in Figure 11*b*, was chosen as the new template. We found 13 intervals that were different from it at the 99% confidence level. No intervals differed significantly from both templates. The temporal pulse shape variations were not clearly correlated with intensity or orbital phase.

In the phase analysis described in § 2.2.1, the same template was used for all outbursts. The template used was generated using DISCLA data which corresponded approximately to combining the first three energy channels in Figure 11*a*. To estimate the effects of pulse shape variations on the orbital model, we first compared the pulse period of 12.3 s to $a_{\rm X}$ sin $i = 128$ lt-s. The pulse period is approximately 10% of $a_{\rm X}$ sin i. Therefore, if the pulse shape variations produced a 0.25 cycle shift in the measured phase (which we think is unlikely), the effect on $a_{\rm X}$ sin i would be only about 2% which is well within our contours. In a system as wide as this one, the effects of pulse shape variations on the orbital solution are fairly small.

Pulse fraction calculations were performed by calculating the mean minus the minimum value for the epoch-folded pulse profiles and dividing that by the average occultation count rate for the interval. Figure 12 shows pulse fractions calculated for five different intervals from seven outbursts. Clearly, the pulse fractions are quite small, $\lesssim 0.15$ for 20–50 keV. Also, the pulse fractions show a marginal increase with energy.

3. DISCUSSION

The most likely scenario describing GS 0834−430 is a Be/X-ray binary with a wide orbit, a small (but nonzero) eccentricity, and a low inclination angle. Figures 8 and 10 rule out a circular orbit. A low inclination angle would give a small mass function and a low pulse fraction (Fig. 12), assuming the spin and orbital angular momentum vectors are aligned. These are both consistent with observations for GS 0834−430. For a typical Be star of 15 $M_\odot$, an inclination angle of 20° gives a mass function of 0.5, which is within the 68% contour in Figure 10. The first nine outbursts were periodic and similar in intensity, consistent with normal (class I; Stella et al. 1986) outbursts observed from other Be/X-ray binaries. In addition, the peak flux (Fig. 3) shows a systematic decline for outbursts 5–9. The last two outbursts (10 and 11) were shifted in orbital phase, with the largest shift occurring for the final outburst. Also, these outbursts did not show the declining intensity trend of the previous five. Thus, the first nine outbursts appear to be related and separate from the last two outbursts. A change in the environment around the neutron star that is not understood apparently occurred between outbursts 9 and 10. GS 0834−430 is unusual because the combination of periodic and aperiodic outbursts with similar intensities has not been observed in other systems. The periodic transient behavior is similar to some Be/X-ray binaries, although no companion has been found. Optical CCD images showed

three stars lying within the *ROSAT* 9″ error circle with $R \lesssim 23.5$ (Belloni et al. 1993). Only the brightest star was studied further, and its spectrum is typical of a normal late-type star. Additional optical and infrared studies are needed to confirm the hypothesis that the companion is a Be star.

Observations of steady spin-up during outbursts allow us to calculate a lower limit to the distance to GS 0834−430 (Chakrabarty et al. 1993). The observed values of the pulsar spin period and derivatives during periods of maximum spin-up imply that $\dot{M} \lesssim 1.1 \times 10^{17}$ g s^{-1}. Combining this with the concurrent 30–100 keV flux observations and the bolometric correction $F_{\rm total} = 3.5 F_{\rm BATSE}$ calculated in § 2.1, we infer that the distance to GS 0834−430 is most likely $\gtrsim 4.5$ kpc.

We close by mentioning two other X-ray binary systems that exhibit characteristics similar to GS 0834−430. The first of these systems provides a possible scenario which would allow a Be companion in a nearly circular orbit. The second system suggests possible transient outburst mechanisms that could allow relatively periodic outbursts that are not dependent on periastron passage. For 2S 1553−542, a system generally accepted as a Be/X-ray binary with a nearly circular orbit, Kelley, Rappaport, & Ayasli (1983) suggest that a small but finite eccentricity could be produced by a supernova explosion involving a small mass loss ($\lesssim 2\ M_\odot$) from a less than 4 $M_\odot$ He star. This model places a mass limit of less than 20 $M_\odot$ on the companion's present mass, allowing a Be companion. GX 301−2, which is a high-mass supergiant system in an eccentric orbit, shows regular near-periastron outbursts and transient weaker apastron outbursts (Pravdo et al. 1995; Koh et al. 1996). Pravdo et al. (1995) suggest that the outbursts occur because the orbital plane of the neutron star and the equatorial disk of material surrounding the companion are misaligned. Perhaps GS 0834−430 outbursts could be described by this model, with a suppression of the secondary outbursts early on followed by an enhancement of these secondary outbursts. Haberl (1991) gives a different possible model for GX 301−2 which consists of a gas stream caused by a region of enhanced mass loss toward the neutron star on the surface of the primary. Outbursts occur when the neutron star passes through the spiral shaped gas stream. Different orbital geometries could change the phases of the outbursts. Perhaps an instability in the gas stream could cause behavior like that seen in the last two outbursts of GS 0834−430. Future observations of GS 0834−430, if it reappears, could improve the orbital parameters and possibly give insight into the behavior of other systems.

This work was supported in part by NASA grant NAG 5-1458. L. B. was supported by the Alfred P. Sloan Foundation. D. C. was supported by a NASA GRSP Graduate Fellowship under grant NGT-51184 and a NASA Compton Postdoctoral Fellowship under grant NAG 5-3109. We thank an anonymous referee for helpful comments.

APPENDIX A

APPENDIX CORRELATIONS DUE TO REBINNING

A pulse profile is easily constructed from a series of photon events by assigning each arrival time t_k a pulse phase according to $\phi(t_k) = \nu t_k \bmod 1$, where ν is the pulse frequency, and by building up an N-bin histogram of phases S_j where $j = 1, \ldots, N$. If the time series is itself binned, one must account for the fact that individual time series bins may overlap more than one pulse profile phase bin. One approach is to treat each time series bin as a delta function at the bin center, and add it entirely into the single appropriate phase bin (*whole bin folding*). While this has the advantage of maintaining statistical independence of the phase bins, it results in some loss of phase information, especially if $1/N\nu \lesssim \tau$, where $\tau = t_{k+1} - t_k$ is the time series spacing. An alternative approach is to split an overlapping time series bin over each of the overlapping phase bins in proportion to the degree of overlap, making the assumption that the accumulated counts were uniformly distributed over the time series bin (*fractional bin folding*). While this will maximally retain phase information, it introduces correlations between phase bins, resulting in apparent fluctuations which can falsely mimic a pulsed signal if not properly accounted for. In this Appendix, we compute the statistical correlations introduced by rebinning.

Consider a binned time series with C_k counts in the kth bin at midtime t_k, with variances σ_k^2 and uniform time spacing τ. We can epoch fold this time series into an N-bin pulse profile with midbin phases $\phi_j = (j + \frac{1}{2})/N$ by computing each phase bin as

$$S_j = \sum_k f_{jk} C_k \,, \tag{A1}$$

where the rebinning factor f_{jk} for fractional bin folding is given by

$$f_{jk} = \frac{1}{\tau} \int_{t_k - \tau/2}^{t_k + \tau/2} F_j(\phi) dt \,, \tag{A2}$$

with

$$F_j(\phi) = \begin{cases} 1 & \text{for } \phi_j - \dfrac{\Delta\phi}{2} < \phi(t) < \phi_j + \dfrac{\Delta\phi}{2} \,; \\ 0 & \text{otherwise} \,, \end{cases} \tag{A3}$$

where $\Delta\phi = 1/N$. {Note that for whole bin folding, $f_{jk} = F_j[\phi(t_k)]$.} Similarly, the integration time accumulated in each phase bin is

$$T_j = \sum_k f_{jk} \tau \,, \tag{A4}$$

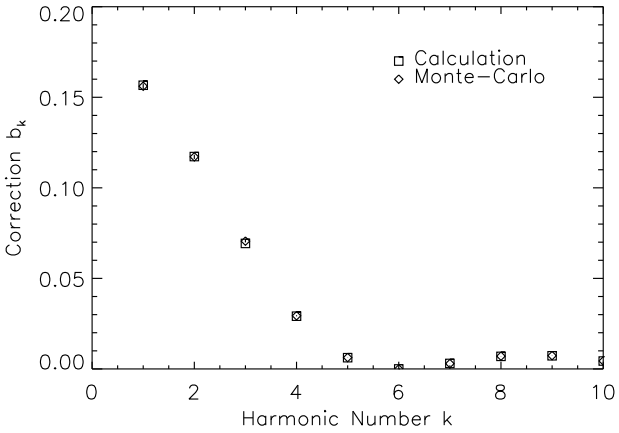

FIG. 13.—Calculated and Monte Carlo simulated values of the rebinning factor b_k used to account for correlations in pulse profiles. The Appendix describes b_k in detail.

so that the count rates in the pulse profile are just $R_j = S_j/T_j$. The square pulse function $F_j(\phi)$ can be represented by the infinite Fourier series,

$$F_j(\phi) = \frac{1}{N} \sum_{m=-\infty}^{\infty} \operatorname{sinc}\left(\frac{m\pi}{N}\right) e^{2\pi i m(\phi - \phi_j)} , \tag{A5}$$

where sinc $x = \sin x/x$ and $i = (-1)^{1/2}$. Since the instantaneous pulse phase is $\phi(t) = \phi(t_j) + \nu(t - t_j)$, where ν is the pulsar spin frequency, the rebinning factor can be rewritten as

$$f_{jk} = \frac{1}{N} \sum_{m=-\infty}^{\infty} \operatorname{sinc}(\pi m \nu \tau) \operatorname{sinc}\left(\frac{m\pi}{N}\right) e^{2\pi i m[\phi(t_k) - \phi_j]} . \tag{A6}$$

The covariance of the pulse profile rates is

$$\operatorname{Cov}(R_j, R_k) = \sum_n \frac{f_{jn} f_{kn} \sigma_n^2}{T_j T_k} , \tag{A7}$$

where f_{jn} and f_{kn} are computed according to equation (A6). If we assume $\phi(t_k)$ is uniformly distributed (which is equivalent to requiring that the length of the time series is $\gg 1/\nu$ and that τ and the pulse period are incommensurate), then the phase-averaged covariance is

$$\operatorname{Cov}(R_j, R_k) = \frac{\sum_n \sigma_n^2}{N^2 T_j T_k} \sum_{m=-\infty}^{\infty} \operatorname{sinc}^2(m\pi\nu\tau) \operatorname{sinc}^2\left(\frac{m\pi}{N}\right) e^{2\pi i m[\phi(t_k) - \phi_j]} . \tag{A8}$$

We can rewrite this in terms of a correlation coefficient,

$$\frac{\operatorname{Cov}(R_j, R_k)}{[\operatorname{Var}(R_j) \operatorname{Var}(R_k)]^{1/2}} = \frac{\sum_{m=-\infty}^{\infty} \operatorname{sinc}^2(m\pi\nu\tau) \operatorname{sinc}^2(m\pi/N) e^{2\pi i m[\phi(t_k) - \phi_j]}}{\sum_{m=-\infty}^{\infty} \operatorname{sinc}^2(m\pi\nu\tau) \operatorname{sinc}^2(m\pi/N)} , \tag{A9}$$

where $\operatorname{Var}(R_j) = \operatorname{Cov}(R_j, R_j)$ is the variance of an individual pulse profile bin.

We are now in a position to examine the statistical behavior of the pulse profile in the frequency domain by means of harmonic decomposition of the pulse. The harmonic coefficients of the pulse profile are

$$a_k = \frac{1}{N} \sum_{j=1}^{N} R_j e^{-2\pi i k \phi_j} , \tag{A10}$$

and the covariance between these harmonic coefficients can be calculated as

$$\operatorname{Cov}(a_k, a_l) = \frac{1}{N^2} \sum_{j=1}^{N} \sum_{m=1}^{N} \operatorname{Cov}(R_j, R_m) e^{-2\pi i (k\phi_j - l\phi_m)} . \tag{A11}$$

Substituting for $\operatorname{Cov}(R_j, R_m)$ using equation (A9), we find

$$\operatorname{Cov}(a_k, a_l) = \delta_{kl} \operatorname{Var}(R_k) \frac{\sum_{j=-\infty}^{\infty} \operatorname{sinc}^2[(k + jN)\pi\nu\tau] \operatorname{sinc}^2[(k + jN)\pi/N]}{\sum_{n=-\infty}^{\infty} \operatorname{sinc}^2(n\pi\nu\tau) \operatorname{sinc}^2(n\pi/N)} , \tag{A12}$$

from which it follows that the harmonic coefficients are uncorrelated and that

$$\sigma^2_{\mathrm{Re}\,(a_k)} = \sigma^2_{\mathrm{Im}\,(a_k)} = \tfrac{1}{2} \operatorname{Var}(a_k) . \tag{A13}$$

We can write the variance of the real part of harmonic coefficient as

$$\sigma^2_{\mathrm{Re}\,(a_k)} = \frac{b_k}{2N}\,\mathrm{Var}\,(R)\,, \tag{A14}$$

where the rebinning correction factor b_k is given by

$$b_k = \frac{N\sum_{j=-\infty}^{\infty}\mathrm{sinc}^2\,[(k+jN)\pi\nu\tau]\,\mathrm{sinc}^2\,[(k+jN)\pi/N]}{\sum_{n=-\infty}^{\infty}\mathrm{sinc}^2\,(n\pi\nu\tau)\,\mathrm{sinc}^2\,(n\pi/N)}\,. \tag{A15}$$

Note that for whole bin folding, $b_k = 1$. For the fractional bin folding of CONT data used to study GS 0834−430 in this paper, we have $N = 64$ phase bins and $\tau = 2.048$ s, and $1/\nu = 12.3$ s. This calculation has been verified by Monte Carlo simulations using these values. The results of the calculation and simulations are shown in Figure 13.

REFERENCES

Aoki, T., et al. 1992, PASJ, 44, 641
Belloni, T., Hasinger, G., Pietch, W., Mereghetti, S., Bignami, G. F., & Caraveo, P. 1993, A&A, 271, 487
Callanan, P. J., et al. 1995, ApJ, 441, 786
Chakrabarty, D., et al. 1993, ApJ, 403, L33
Corbet, R. H. D. 1986, MNRAS, 220, 1047
Deeter, J. E., Boynton, P. E., & Pravdo, S. H. 1981, ApJ, 247, 1003
Denis, M., et al. 1993, A&AS, 97, 333
Fishman, G. J., et al. 1989, in Proc. GRO Science Workshop, ed. W. N. Johnson (Greenbelt: NASA/GSFC), 2
Grebenev, S., & Sunyaev, R. A. 1991, IAU Circ. 5294
Haberl, F. 1991, ApJ, 376, 245
Harmon, B. A., et al. 1992, in Compton Observatory Science Workshop, ed. C. R. Schrader, N. Gehrels, & B. Denis, NASA Conf. Publ. 3137, 69
Kaniovskii, A. S., et al. 1994, Astron. Lett., 20, 207
Kelley, R. L., Rappaport, S., & Ayasli, S. 1983, ApJ, 274, 765
Koh, D. T., et al. 1996, ApJ, submitted
Lampton, M., Margon, B., & Bowyer, S. 1976, ApJ, 208, 177
Lapshov, I. Yu., Dremin, V. V., Sunyaev, R. A., Brandt, S., & Lund, N. 1992a, Soviet Astron. Lett., 18, 12
Lapshov, I., Dremin, V. Sunyaev, R., Yascovich, A., Brandt, S., Castro-Tirado, A. J., & Lund, N. 1992b, private communication
McNamara, B. J., Harmon, B. A., & Harrison, T. E. 1995, A&AS, 111, 587
Pravdo, S. H., Day, C. S. R., Angelini, L., Harmon, B. A., Yoshida, A., & Saraswat, P. 1995, ApJ, 454, 872
Robinson, C. R. 1996, private communication
Standish, E. M., Newhall, X. X., Williams, J. G., & Yeomans, D. K. 1992, in Explananatory Supplement to the Astronomical Almanac, ed. P. K. Seidelmann (Mill Valley, CA: University Science), 279
Stella, L., White, N. E., & Rosner, R. 1986, ApJ, 308, 669
Sunyaev, R. A. 1991, IAU Circ. 5180
Sunyaev, R. A., Grebenev, S., Denis, M., & Goldwurm, A. 1992, IAU Circ. 5437
Waters, L. B. F. M., de Martino, D., Habets, G. M. H. J., & Taylor, A. R. 1989, A&A, 223, 207
Waters, L. B. F. M., & van Kerkwijk, M. H. 1989, A&A, 223, 196
Wilson, C. A., et al. 1994, in AIP Conf. Proc. 308, The Evolution of X-Ray Binaries, ed. S. S. Holt & C. S. Day (New York: AIP), 259